



e-ISSN No.: 2582-4228

Journal of Indian Association for Environmental Management

Journal homepage: [www.http://op.niscair.res.in/index/php/JIAEM/index](http://op.niscair.res.in/index/php/JIAEM/index)



Rejection Behaviour of Manganese Ions from Synthetic Wastewater by Nanofiltration Membrane

Pratiksha Patil^a, Jotiram G. Gujar^a, Sanjay M. Chavan^a, Shriram S. Sonawane^b

^aSinhgad College of Engineering, Department of Chemical Engineering, S. No. 44/1, Off. Sinhgad Road, Pune, 411041, India.,

^bVisvesvaraya National Institute of Technology, Department of Chemical Engineering, S Ambazari Rd, Ambazari, Nagpur, 440010, India.

jotiramgujar@gmail.com, jggujar.scoe@sinhgad.edu, shriramsonawane@gmail.com

Submitted: **October 29, 2020**

Revised: **January 13, 2021**

Accepted: **January 27, 2021**

Abstract: Because of the development of novel applications, nanofiltration has attracted much interest in recent years. This research describes the removal of manganese ions from synthetic wastewater using a TFC NF-30 membrane. The effects of different operating parameters on heavy metal rejection were investigated, including feed concentration (20-60 ppm), applied pressure (5-8 kg/cm²), and pH (4-6). According to the current findings, the rejection coefficient for manganese ions increases with increasing pressure. The rejection coefficient reduces as the feed concentration of manganese ions increases at a steady flow rate.

The influence of pH was investigated, and it was discovered that when the pH rises, the rejection of manganese ions rises as well. The maximum measured metal rejection is reported to be 99.03 percent to 96.88 percent, for an initial feed concentration of 20 ppm and 40 ppm. The experimental data were fitted with membrane transport models such as combined-film theory-Spiegler-Kedem (CFSK) for the evaluation of the membrane transport parameters and mass transfer coefficient, *k*. For manganese ions, CFSK models were applied to estimate the experimental rejection (*R_{OE}*) or actual rejection and modeling rejection (*R_{OM}*) or observed rejection. In the CFSK model, the experimental and modeling rejection for manganese is roughly identical to ± 0.03 .

Keywords: Nanofiltration, manganese, rejection, membrane transport model, CFSK model

I. INTRODUCTION

Heavy metal contamination is now a major source of concern for environmentalists. Manganese is a typical heavy metal pollutant of wastewater and groundwater since it is a major industrial raw material. Geochemical processes and human activities emit a large number of toxic compounds into the environment, like manganese (Mn), cobalt (Co), copper (Cu), zinc (Zn), and, iron (Fe), contaminating water [1,2] and decreasing the effectiveness of water remediation strategies [3]. The existence of manganese (Mn²⁺) in drinking water not only generates a steel flavor in the water but also causes pipe obstruction [4]. Manganese overdose has been identified as a major threat to human fitness [5]. Manganese removal from water is frequently accomplished via aeration-sand filtration [6-7]. Fe and Mn concentrations in drinking water should be substantially less than zero, according to the World Health Organization. 3mg/L and 0.01%, respectively [8]. The natural occurrence of Fe and Mn in groundwater occurs when it is

very little or no oxygen present, usually in deeper wells, in places where groundwater drift is sluggish, and in areas where groundwater runs through soils rich in natural matter. Fe and Mn are commonly found in natural groundwater as divalent ions, Fe²⁺ and Mn²⁺, in their most soluble form. They are colorless in soluble form in groundwater, but when exposed to air, they oxidize and transform into insoluble Fe³⁺ and Mn⁴⁺, respectively, leaving the water with a brown-red color. To remove these metals from groundwater, many procedures were used, including ion-exchange and water softening, activated carbon adsorption, aeration and filtration, biosorption, ionic liquid extraction, and so on [9-13].

It is observed that this sort of lined film should be freshly covered across the exterior of the sieve components (i.e., quartz sand and anthracite) regularly, in addition to manganese removal by automobile-catalytic techniques employing non-stop produced MnOx [14]. However, forming an "energetic covered movie" on the floor of virgin sand for efficient

manganese separation through the aeration-sand filtering operation typically takes a long time (months) [15]. For this purpose, a strong oxidizing agent like potassium permanganate (KMnO_4), chlorine dioxide (ClO_2), ozone (O_3), or other industrially utilized oxidants [16-17] can be employed to speed up the creation and development of the spark off coated movie formed across the exterior of virgin quartz gravel [18].

Iron and manganese, which are typically found in natural groundwater [19], can produce aesthetic and operational issues, as well as unpleasant flavor and shade, as well as health problems in water resources [20]. In the case of separation of manganese and iron from groundwater in domestic water transport methods, a variety of treatment options have been examined [21-22], including physical, chemical, physicochemical, and organic approaches. Because Mn^{2+} is more difficult to oxidize than Fe^{2+} due to manganese's higher redox capacity, effective separation of Fe and Mn from groundwater continues to be a challenge. Haddadi et al. investigated the kinetics and isotherms of boron adsorption from water using titanium dioxide extensively. Pseudo-first order, pseudo-second-order, reversible first order, and Elovich kinetic models were used to describe the equilibrium data [23]. Aeration and/or chemical oxidants such as chlorine dioxide, chlorine, hypochlorite, potassium permanganate, or ozone, were previously used to oxidize Fe and Mn in groundwater [24]. In recent years, however, membrane techniques combined with peroxidation have been gradually investigated to meet the additional strict water quality criteria with the present device.

Microfiltration (MF) with aeration and NaOCl oxidation UF using pre-chlorination [25-26], a polymeric and ceramic UF membrane technique in addition to pre-oxidation [27-28]. Mn-oxidizing microorganisms (MnOB) are frequently preferred over Mn-lowering bacteria to speed up birnessite production. As a result, creating favorable conditions for MnOB development is a critical aspect of operations. MnOB enrichment can also be improved by adopting a good strong-liquid separation method. Ultrafiltration membranes have been well-known for their ability to effectively listen to microorganisms at various stages of the filtration system [29-30]. As a result, adding ultrafiltration into birnessite-based water treatment is excellent for manganese elimination and biofilm development. A manganese oxide-containing catalytic clay membrane has previously been investigated [31]. A clay membrane device coupled with peroxidation proved active in manganese regulators in the feed solution, according to Kenari et al. [32]. They also created a pyrolusite fluidized bed with a ceramic membrane device to help remove manganese from drinking water [33]. The auto-catalytic/oxidation character of continually designed birnessite was neglected in these studies, this was the impetus for the chemical oxidation of manganese preceding membrane cleaning.

Membrane technology is generally regarded for treating groundwater, saltwater, brackish and well water, and industrial wastewater [34-35] among many methods. Pressure-driven membrane processes comprise microfiltration, ultrafiltration, nanofiltration, and reverse osmosis [36]. The molecular size of

the contaminants contained in the wastewater determines which accurate procedures to use. Nanofiltration (NF) is a membrane technique that sits between reverse osmosis and ultrafiltration. It effectively removes the substances that cause water hardness, such as calcium and magnesium, as well as germs, viruses, and color [37]. Gadhe et al., also developed various nanotechnology-based strategies for wastewater treatment. They used nickel and hematite nanoparticles for wastewater treatment. [38-40] Authors also emphasized the role of ultrasonic treatment of the nanoparticles for wastewater treatment. [41-44] to Gülsev Soysüren et al [45] studied the elimination of manganese (II) from an aqueous medium by employing ionic liquid-infused polymeric adsorbent and electrode ionization (EDI) methods extensively. To separate manganese (Mn^{2+}) from hydrated solutions, ionic liquid-infused polymeric adsorbent (ILIS) and electro-deionization (EDI) techniques were utilized in this study. The influence of sorbent dosage, starting solution pH, and interaction time on Mn^{2+} separation was investigated. The exclusion of Mn^{2+} by ILIS is Ph-relying, with maximal release at about pH 9.

This study aimed to investigate manganese separation by nano-filtration modules under different operating conditions. The effect of various parameters like pressure, Ph, feed concentration, etc. for the separation of manganese by using a nano-filtration module has been studied. The various affecting parameters were evaluated through the combined-film theory-Spiegler-Kedem (CFSK) model. The experimental data was fitted very well with the CFSK model. As a result, the findings of this study may be used to build a manganese ion removal process that is both environmentally safe and cost-effective for use in water treatment technologies.

II. MATERIALS AND METHODS

Synthetic wastewater samples are constructed using distilled water and sufficient concentrations of manganese (II) sulfate monohydrate ($\text{MnSO}_4 \cdot \text{H}_2\text{O}$). Several replies are grouped with high amounts of manganese (II) sulfate monohydrate (20-60 ppm). The experiments were carried out on a Parma® pilot-scale setup. (Perm Ionics, Vadodara, India). Perma-TFCNF300, an industrial thin-movie composite polyamide membrane, is used to finish the experiments. Inside the experiment, a rectangular flat membrane is employed.

Nanofiltration

A multifunctional filtration method is termed nanofiltration. Membranes with nanometer-sized holes are referred to as NF membranes. At neutral pH, typical NF membranes have a horrible surface rate, which explains why multivalent, negatively charged ions are rejected better [46-51]. Because the micropore diameter (DP) of the NF membrane is much smaller than 2 nm, it is possible to accurately remove divalent and few single valet ions, solubilized organics (molecular weight Mw 200-500 g/mol), hardness, and heavy substances. Currently, Thin Film Composite (TFC) membranes were industrially operative membranes for various manufacturing separation operations, especially water handling and decontamination methods [52-56].

Experimental Set-Up and Procedure

The investigations were carried out in a quadrilateral plane membrane cell. The membrane-housing cell (Figure 1) was prepared with stainless steel and has two sections that are linked together with high-tensile fasteners. The waft distribution chamber is located in the top half of the cell, while the membrane support system is located in the bottom half. The membrane needs assistance to prevent it from rupturing at

greater hydrostatic pressures. The following unique help arrangements were used, mm thick perforated chromium plate is placed on a 300 mesh stainless steel sensor covered with Whatman filter paper, stalked by a real membrane across an active thin-film open to a large voltage fluid. At high pressures, this configuration gives enough mechanical balance for the test diaphragm. The overhead half of the observation chamber has a canal for attaching an HDPE O-ring to lower the outflow during heavy-load processes [57].

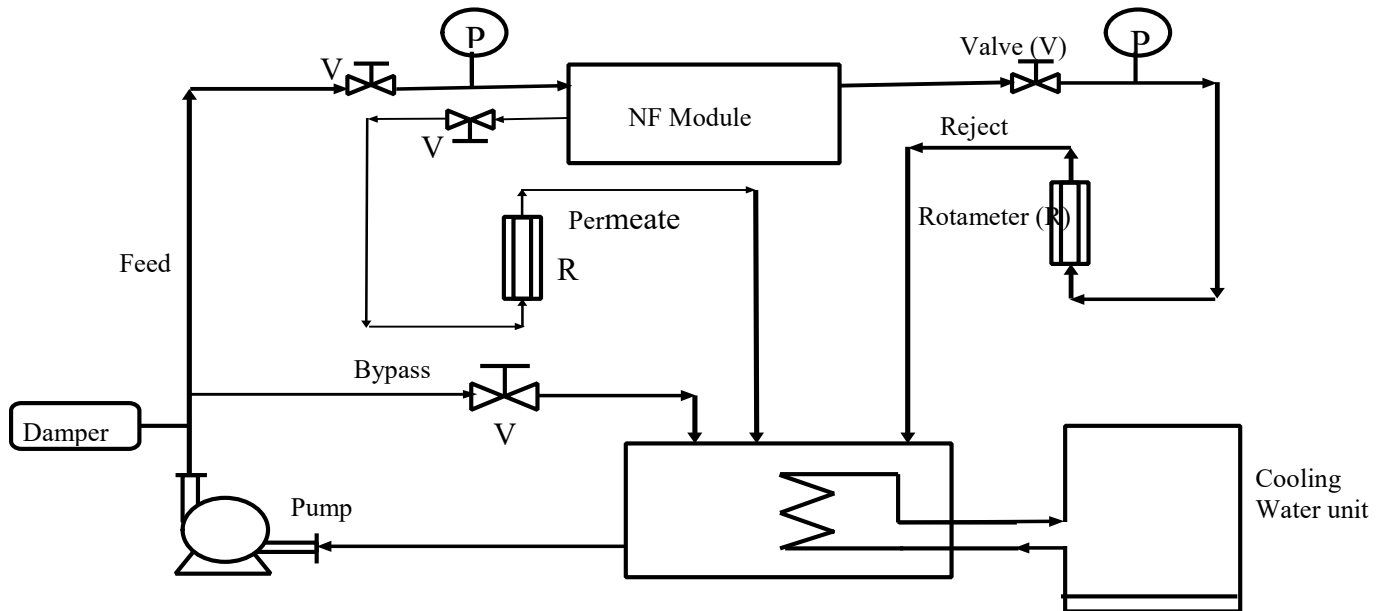


Figure 1: Schematic diagram of Perma® pilot-scale membrane system

Experiments were conducted on Perma- TFC-NF-three hundred (Permionics, Vadodara, India), also known as NF-three hundred membrane, a commercial skinny-movie composite polyamide membrane. This membrane is made up of three coatings. The initial part is a polyamide polymer with a thickness of five to twenty meters that performs the real removal process. The middle part is comprised of polysulfone with a thickness of 50 micrometers. The last part, which is utilized to test resistance and energy, is formed by polyester and has a width of around 150 m. Perma-TFC membranes can endure pH ranges of 2–12, pressures and temperatures of about 30 atm, and up to 50 °C respectively.

The 300 Da cut-off is used to describe the NF-three hundred membrane. The surface area of the strong membrane is 150 cm². The system will be able to manage the concentration polarization because of the 1mm thin opening within the membrane check cell and the excessive pass-waft concentrate employed in the experiment. Before performing the real tests for manganese ion rejection, the NF-three hundred membrane is stabilized for 2 hours at 20 atm, which is the highest stress employed in the studies, to regulate required membrane compaction while experimenting.

Experiments were conducted in batch move mode for two hours for each set of rejection facts and permeate samples were gathered from extreme strain to minimize pressure for certain initial parameters and input discharge. To maintain

consistent feed awareness, each permeate and concentrate is reverted to the input feed vessel. Permeate samples are taken at a certain time c language to assess the salt rejection (Ro) and permeate volumetric flow (Jv). According to traditional methods, manganese ion concentrations were determined using an atomic absorption spectrophotometer. To smooth the device, the module is cleaned with distilled water for 30 minutes at 4 atm every after a set of experiments for a certain initial concentration [58].

Method of Analysis

The manganese ion concentrations were determined by using an atomic absorption spectrophotometer (version SL-173). A little quantity of the sample is introduced into a flame, which reduces the ions to elements and causes them to evaporate. The components in the sample absorb light at different wavelengths in the visible and ultraviolet spectra. A monochrome detects a light beam directed through the flame with a single unique wavelength for the detail measured. To quantify the fundamental concentrations, the mild absorbed by the extract-containing flame is compared to the absorption from considered requirements. Before the evaluation, samples with excessive amounts of elements beyond the tool's linear range must be diluted. To evaluate the unknown concentration of manganese in the solution, a calibration curve was utilized. The unknown solution was supplied to the instrument, and the detail of this solution absorbance was measured. The

calibration curve is then used to compute the unknown concentration of the manganese.

The membrane's total performance is now evaluated in terms of membrane rejection R. (percent). The selectivity of a membrane for dilute aqueous mixes including water and a solute is usually described in terms of the found solute rejection coefficient. This parameter is a measure of the membrane capacity for separating the solute from the feed solution, and it may be calculated using the equation below:

$$R_o = \left(1 - \frac{C_p}{C_f}\right) \dots\dots\dots(1)$$

Where,
 C_p represents the concentration of the particle component in permeate.
 C_f is its feed concentration.

concentrations of 20ppm, 40ppm, and 60ppm. Special operating conditions were used in the experimental runs.

1. The calculation for observed rejection

The film idea version calculates the rejection of manganese ion from manganese (II) sulfate monohydrate salt as,

$$R_o = \left(1 - \frac{C_p}{C_f}\right)$$

Where,
 C_p is the concentration of permeate
 C_f is the concentration of the feed

Effect of feed concentration on rejection

Experiments were performed to study the influence of feed concentrations of 20 ppm, 40 ppm, and 60 ppm on manganese ion rejection for extreme applied stress at different pH levels of 4, 5, and 6. The experimental runs lasted 20 minutes, and samples were collected and analyzed by using AAS every five minutes.

III. RESULTS AND DISCUSSION

To understand the performance of the nano-filtration module, an analytical model was used. The wastewater samples were created synthetically by adding manganese (II) sulfate monohydrate ($MnSO_4 \cdot H_2O$) to distilled water in

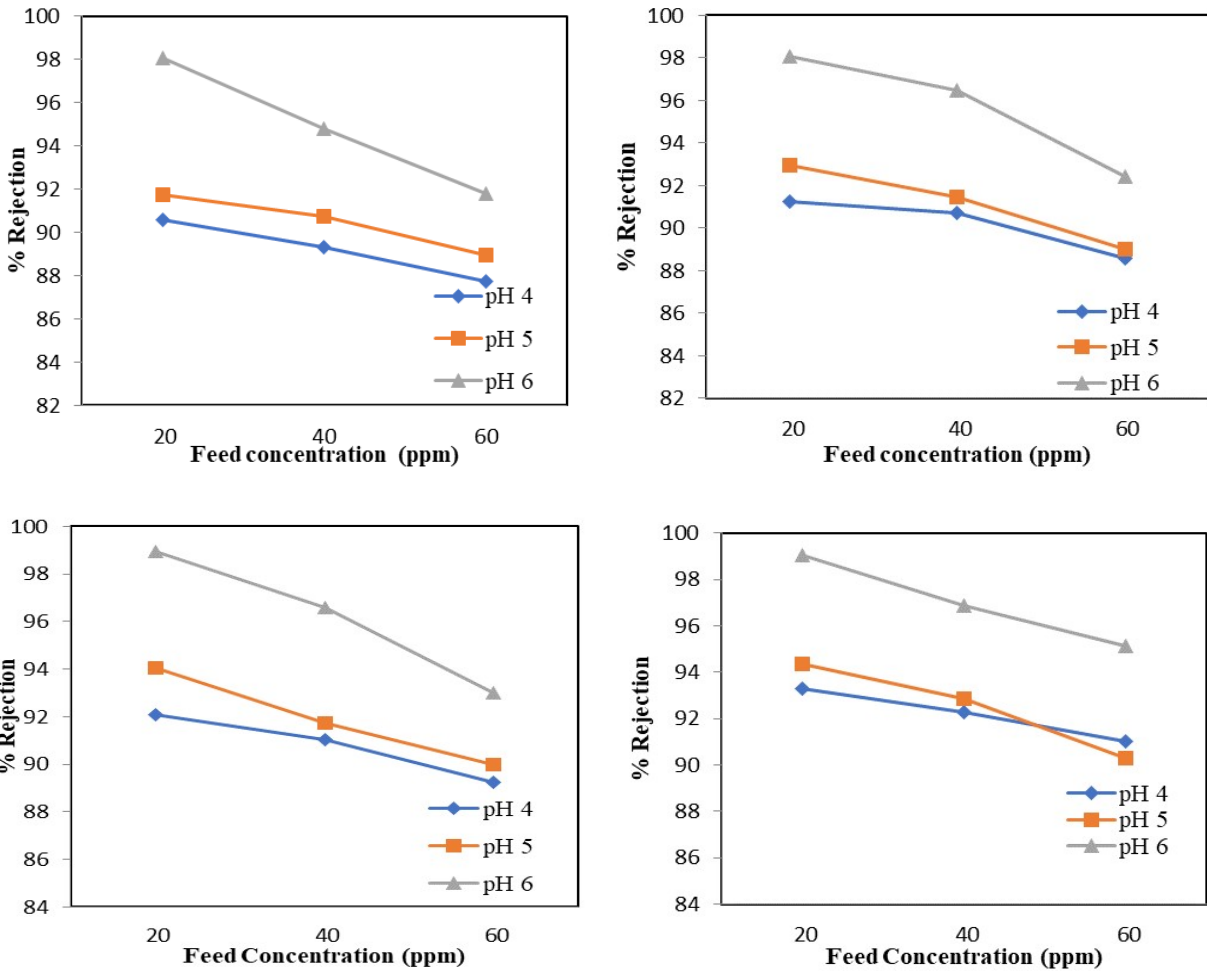


Figure 2: % Rejection Vs Feed concentrations (C_f) for different pH & different pressure (a) $P= 5 \text{ kg/cm}^2$, (b) $P= 6 \text{ kg/cm}^2$, (c) $P= 7 \text{ kg/cm}^2$, (d) $P= 7 \text{ kg/cm}^2$

The manganese ions rejection decreases as the feed concentration increase on every factor of time, as shown in Figure 2. This type of behavior might be fairly prevalent. As the knowledge of solutions grows, so does the awareness of solutes across the membrane exterior, resulting in the formation of a layer of concentration polarization. At the same time, another occurrence is noticed with a surge in feed attention, and it's the result of osmotic pressure. The type and concentration of salts or organics in feed water is a characteristic of osmotic pressure.

With increasing feed concentration, there was a rise in solute attention inside the reject water, especially on the membrane wall, increasing osmotic pressure. As the osmotic pressure of a solution rises, it tends to waft more solvent into the permeate aspect, lowering the rejection coefficient. As a result, permeating attention is reduced, and the rejection coefficient lowers as feed awareness is doubled. Z.V.P. Murthy et al [59] found comparable results for nickel ions while R. R. Bhutale et al found similar results for chromium ions separation [60].

Effect of applied Pressure on rejection

These tests were carried out to see how pressure applied at rates ranging from 5 to 8 kg/cm² affected manganese ion rejection for extraordinary feed attention. The experimental runs were completed for 20 minutes, and samples were

evaluated on AAS for 5 minutes at a time, with the following readings:

Figure 3. shows that the rejection of manganese ions increases as the pressure rises at each stage of the separation. This finding was reached because convectonal ion transport becomes more significant than diffusion. Due to enhanced convective flux, when pressure rises, the greatest amount of solvent goes through the membrane pores. As a result, the solute concentration in permeate is diluted. Low retention at reduced pressure is due to the low diffusive transport of manganese ions over the membrane in contrast to convective transport.

Convective solvent transportation is becoming increasingly important as stress levels rise. As a result, with increased strain, the retention coefficient will increase.

Effect of Ph on rejection

Experiments are being conducted to determine the influence of Ph 4, 5, and 6 on manganese ion rejection for various feed concentrations and pressures ranging from 5 to 8 kg/cm². The experiments lasted 20 minutes, and samples were checked on AAS every 5 minutes, with the following readings:

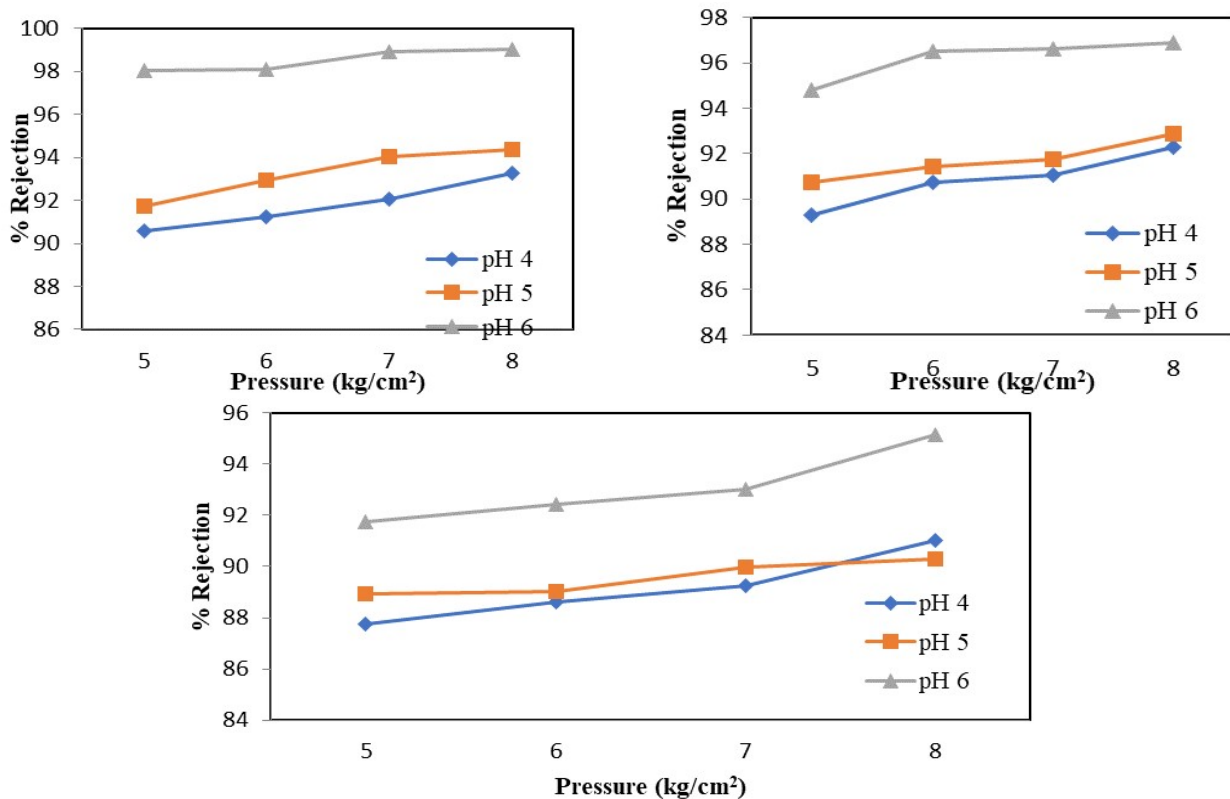


Figure 3: % Rejection Vs Pressure for different Ph & different feed concentrations (a) C_f = 20 ppm, (b) C_f = 40 ppm (c) C_f = 60 ppm

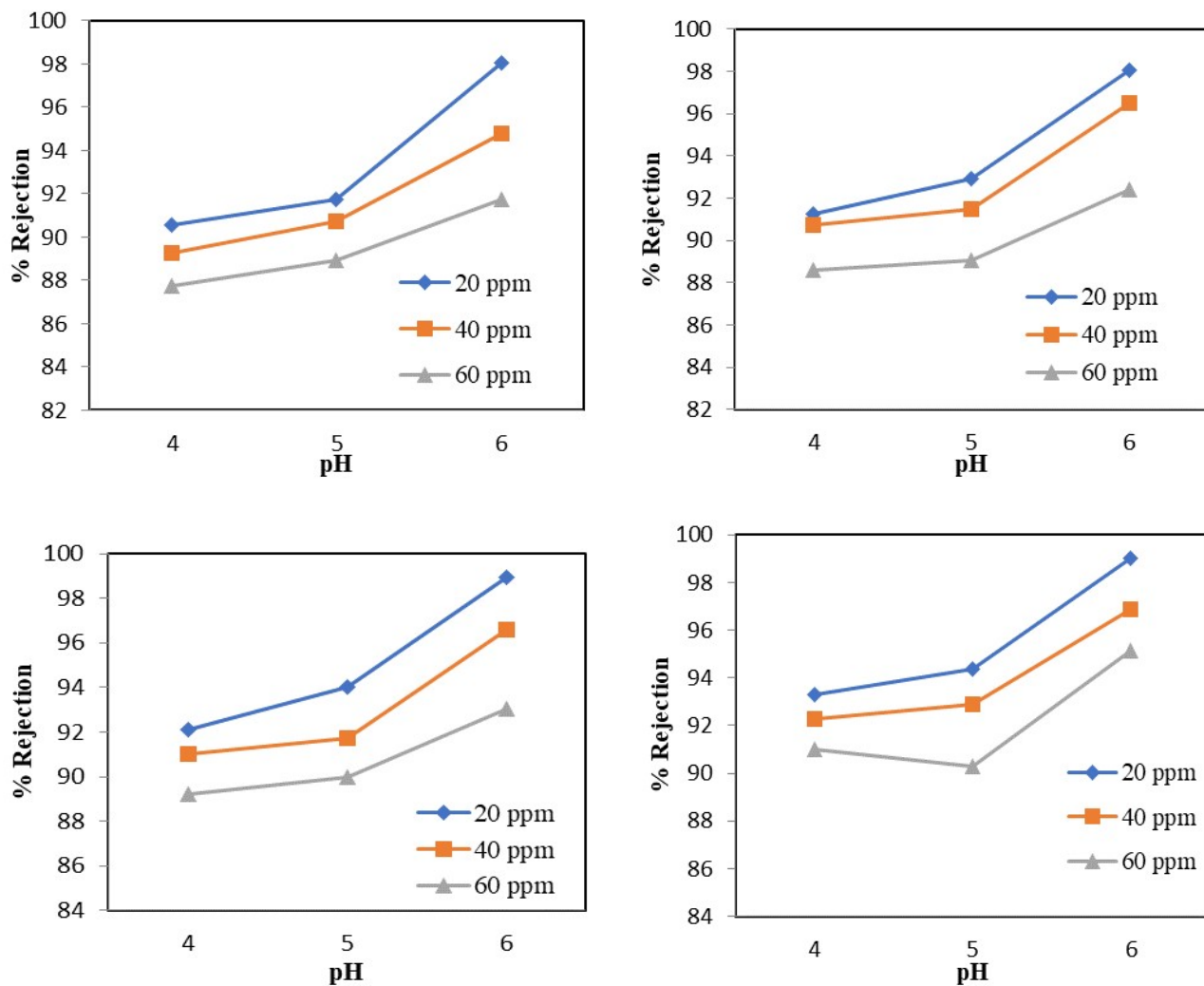


Figure 4: % Rejection Vs Ph for different feed concentrations (C_f) & different pressure (a) $P=5 \text{ kg/cm}^2$, (b) $P=6 \text{ kg/cm}^2$, (c) $P=7 \text{ kg/cm}^2$, (d) $P=8 \text{ kg/cm}^2$

The manganese ions rejection increases with the increase in feed answer Ph up to Ph 6 as shown in Figure 4. A higher Ph within the initial solution aided the conversion of soluble divalent Mn^{2+} ions to Mn^{4+} ions, which were more powerful and precipitated without difficulty on membrane surfaces. The solubility of divalent metallic ions (Mn^{2+}) has reduced as the Ph of the feed solution has increased. As a result of the improved Ph in the feed solution, metal ions flocculated, resulting in greater rejection of steel components from synthetic wastewater. For Iron and Manganese ions, the same results were found with the help of Norherdawati Kasim et al [61].

Effect of pressure on permeate flux

Experiments were conducted to investigate the influence of applied pressures from 5 to 8 kg/cm^2 on permeate flux over the long term, at various Ph(4,5,6) and feed concentrations. The experimental runs lasted 20 minutes, and samples were analyzed on AAS every five minutes.

The permeate flow increases as the pressure increases. The convective transport and awareness polarization become increasingly essential as stress levels rise. This shows that the permeate flow alternates with increasing pressure but remains linear, indicating minor consciousness polarization. B.A.M. Al-Rashdi et al [62] reported equivalent effects for Cd (II), Cu (II), Mn (II), and Pb (II) ions while Bhutale et al [60] showed analogous effects for chromium ions separation [63].

Because the permeate flux accelerated, the rejection became seen to grow with a linear courting, as shown in Figure 6 for manganese.

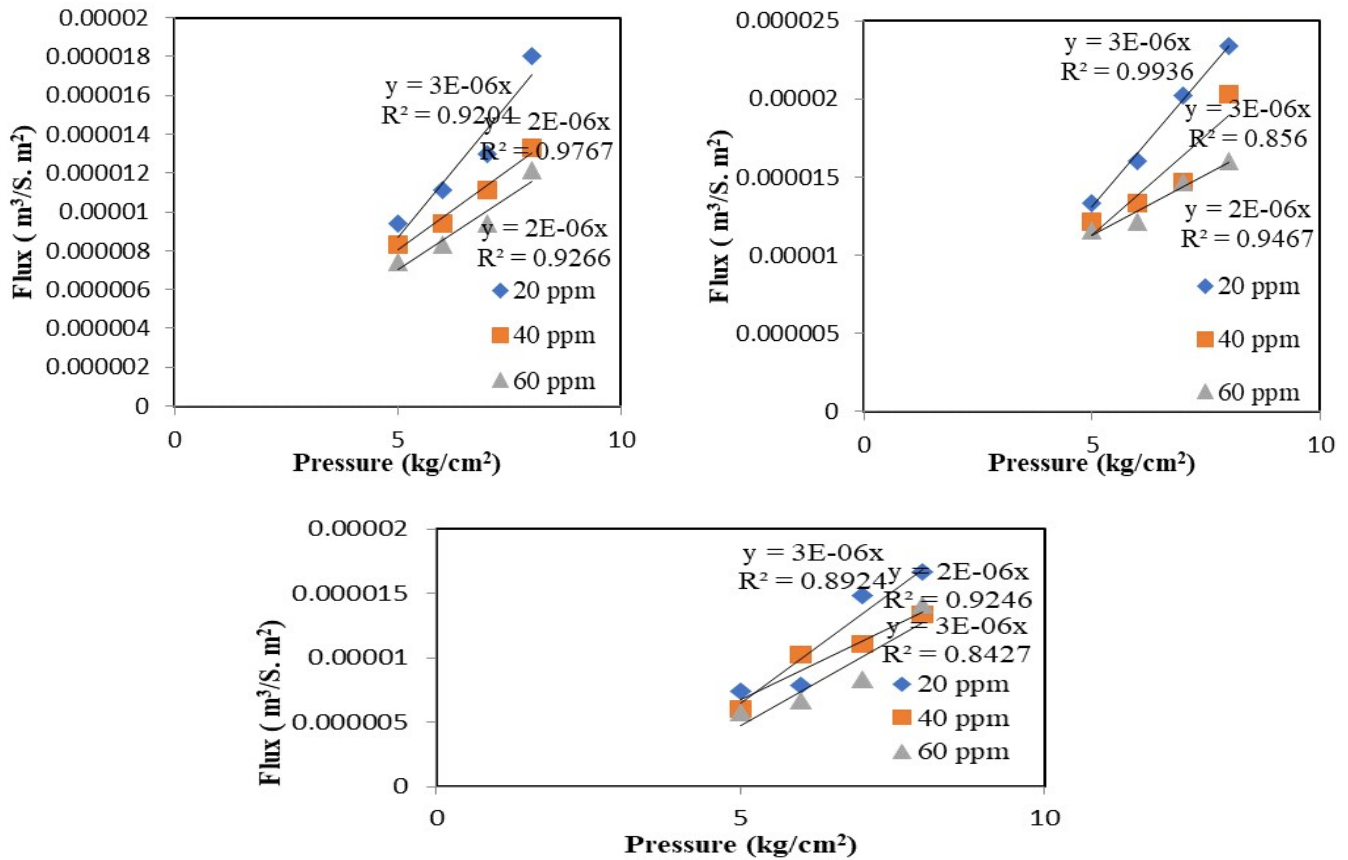


Figure 5: Permeate Flux Vs Pressure for different feed concentrations (C_f) & various Ph
(a) Ph = 4 (b) Ph = 5 (c) Ph = 6

Combined-film theory-Spiegler-Kedem model

$$a_2 = \frac{1-\sigma}{PM} \dots\dots\dots(6)$$

The basic equations of the solution-diffusion model [64] can be written as

$$J_v = A (\Delta P - \Delta\pi) \dots\dots\dots(1)$$

$$J_A = \left(\frac{D_{AM}K}{\delta}\right)(C_{A2} - C_{A3}) \dots\dots\dots(2)$$

Where A is the solvent's permeability parameter, which may be determined using purified water permeability experiments. The solute transport parameter ($\frac{D_{AM}K}{\delta}$) is regarded as a single parameter.

The nonlinear Spiegler-Kedem model's working equations are as follows:

$$J_v = L_p (\Delta P - \sigma \Delta\pi) \dots\dots\dots (3)$$

$$R = \frac{\sigma(1-F)}{(1-\sigma F)} \dots\dots\dots(4)$$

Where,

$$F = \exp [-J_v a_2] \dots\dots\dots(5)$$

with

Here, is a reflection coefficient that defines a membrane's rejection capacity, where = 0 implies no rejection and = 1 means 100% rejection, PM is the overall permeability coefficient, and L_p is the membrane's hydraulic permeability coefficients, which are identical to a provided Eq (1). It's possible to rearrange Eq. (2) to get

$$\frac{k}{L_p} = a_1 (1-F) \dots\dots\dots (7)$$

Where

$$a_1 = \frac{\sigma}{1-\sigma} \dots\dots\dots(8)$$

$$\frac{R_Q}{(1-R_Q)} = \left[\frac{R}{(1-R)} \right] \left[\exp \left(\frac{-J_v}{k} \right) \right] \dots\dots\dots (9)$$

The aforementioned equation, together with a suitable mass transport equation for the membrane, may now be utilized to calculate the membrane properties as well as the mass transfer coefficient k [65].

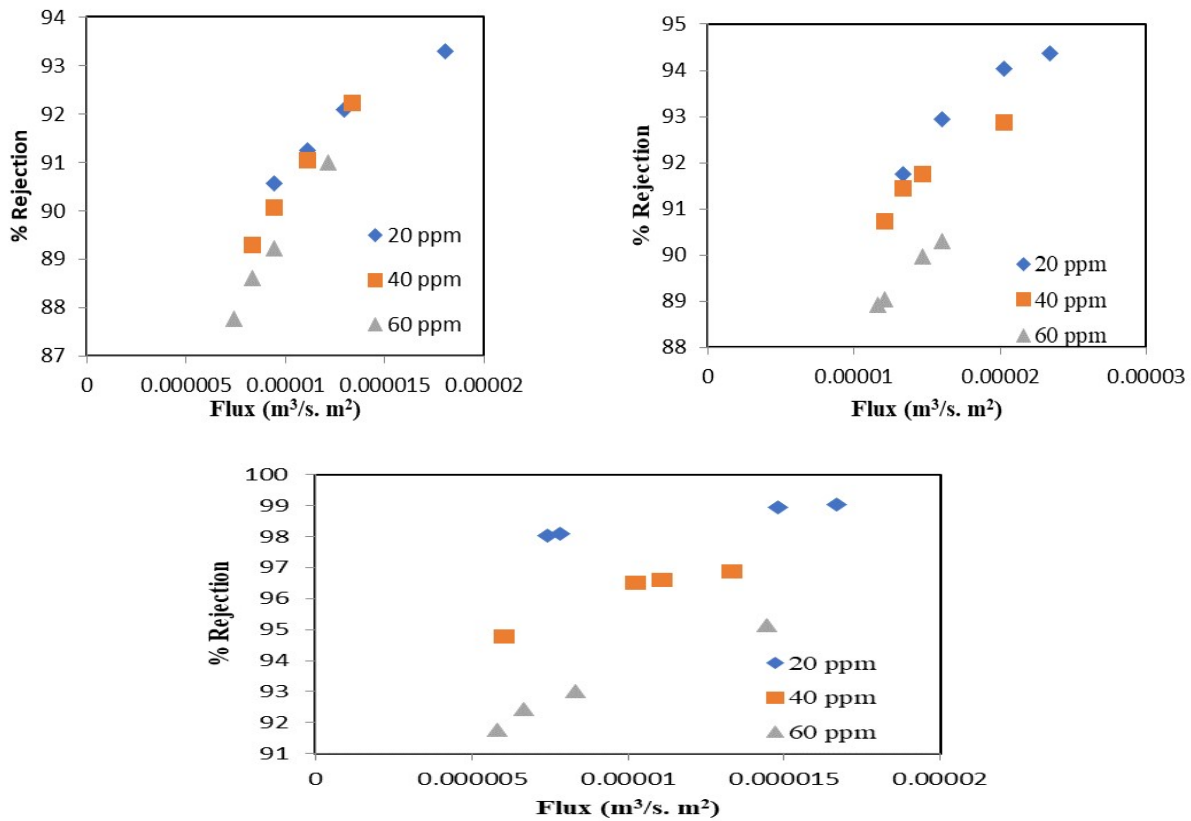


Figure 6: % Rejection Vs Permeate flux for different feed concentrations (C_f) & various Ph (a) Ph = 4 (b) Ph = 5 (c) Ph = 6

Now, the putting Equation (7) into Equation (9) gives the subsequent equation:

the second is convective transport. As a result, the equation may be expressed as follows:

$$J_S = J_V \cdot C_P = J_{diff} + J_V \cdot C_{Conv} \dots\dots\dots(13)$$

$$\frac{Ro}{1-Ro} = a_1 [1 - \exp(-J_V \cdot a_2)] \left[\exp\left(-\frac{J_V}{k}\right) \right] \dots\dots\dots(10)$$

With $J_{diff} = P_S (C_m - C_p)$ and $C_{conv} = (1-\sigma) C_{int}$, by dividing equation (11) with J_V we obtain:

$$C_p = J_{diff} \frac{1}{J_V} + C_{Conv} \dots\dots\dots(14)$$

The working equation for the combination-film theory-Spiegler-Kedem (CFSK) model is Eq (10). Using the nonlinear parameter estimation technique, we can estimate the membrane parameter and PM, as well as the mass transfer coefficient k , simultaneously by submitting data of Ro vs. J_V taken at different pressures, but at constant feed rate and constant feed concentration for each set. Figure 7 depicts the % rejection and permeate flux.

The slope of this equation C_p Vs $1/J_V$ corresponds to the diffusive flux of salts J_{diff} , while the intercept C_{conv} relates to the salts concentration in permeate transported by convection.

Hydraulic permeability is a parameter that describes how productive a membrane is. The hydraulic permeability of pure water to a membrane, which is based on Darcy's law, displays the permeate flow as a function of the applied pressure [66-67]:

$$J_S = P_S (C_m - C_p) + (1 - \sigma) J_V C_m \dots\dots\dots(11)$$

The equation of the boundary layer theory is expressed by the following relation:

$$J_V = L_p \Delta P \dots\dots\dots(15)$$

$$\frac{C_m - C_p}{C_p - C_p} = \exp\left(\frac{J_V}{k}\right) \dots\dots\dots(12)$$

The word C_o refers to the amount of salt in the diet. There are two terms in equation (9): the first is diffusive transport, and

TABLE 1
Observed Rejection from experiment and modeling at different concentrations and different Ph

Ph	Feed Concentration (ppm)	20 ppm		40 ppm		60 ppm	
		R_{OE}	R_{OM}	R_{OE}	R_{OM}	R_{OE}	R_{OM}
Ph 4	5	0.905	0.907	0.8929	0.895	0.8775	0.8811
	6	0.912	0.914	0.9007	0.900	0.8860	0.8877
	7	0.920	0.919	0.9104	0.907	0.8923	0.8937
	8	0.932	0.928	0.9228	0.913	0.9100	0.9042
Ph 5	5	0.917	0.921	0.9072	0.911	0.8893	0.8901
	6	0.929	0.926	0.9145	0.914	0.8903	0.8921
	7	0.940	0.931	0.9175	0.917	0.8997	0.8996
	8	0.943	0.934	0.9287	0.926	0.9029	0.9025
Ph 6	5	0.980	0.981	0.9478	0.946	0.9177	0.9037
	6	0.980	0.981	0.9650	0.963	0.9243	0.9144
	7	0.989	0.985	0.9660	0.965	0.9301	0.9288
	8	0.990	0.986	0.9688	0.969	0.9514	0.9531

It can be seen from (table 1) that the R_{OE} and R_{OM} values were almost identical. Figures 7. Show a plot of R_{OE} and R_{OM} for feed concentrations of 20ppm, 40ppm, and 60ppm at Ph 4, 5, and 6, with R_2 values close to 1.

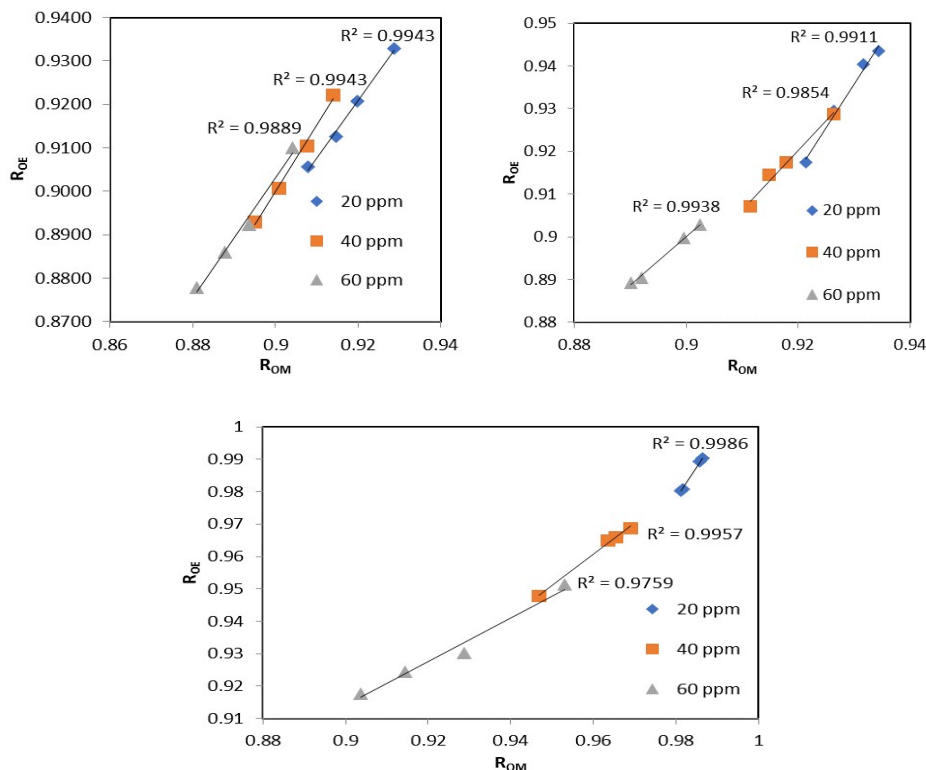


Figure 7: Experimental Observed Rejection vs. Modeling Observed Rejection & various Ph
(a) Ph = 4 (b) Ph = 5 (c) Ph = 6

The membrane performance was predicted using the calculated parameters from the CFSK model. The anticipated values were quite close to the experimental findings [68].

TABLE 2
Parameter estimated using nonlinear techniques for manganese salt from CFSK Model

Ph	Feed Concentration (ppm)	σ	P_M (10^{-7} m/s)	k (10^{-5})
Ph 4	20 ppm	0.9511	-4.0960	-3.2340
	40 ppm	0.9449	-4.1887	-3.9020
	60 ppm	0.9402	-4.4158	-4.1020
Ph 5	20 ppm	0.9512	-4.0447	-3.9000
	40 ppm	0.9480	-4.4893	-4.2100
	60 ppm	0.9345	-5.2020	-4.3100
Ph 6	20 ppm	0.9901	-6.8800	-3.0200
	40 ppm	0.9874	-2.4840	-3.3200
	60 ppm	0.9857	-4.7890	-4.6900

A nonlinear estimating approach may be utilized to evaluate the factors, P_M , and k (Table 2). We employed the least-squares approach in our situation, which allowed us to get a better fit of the theoretical curve between the retention salts and the solvent flow. Y. A. Baussouga et al. obtained similar findings for various salts such as NaCl, Na₂SO₄, and MgSO₄ [69].

TABLE 3

1/Jv Vs Cp at different pressure, different feed concentrations, and different Ph

Ph	Concentration (ppm)	20 ppm		40 ppm		60 ppm	
		1/Jv (10 ⁵) (s.m ² /m ³)	Cp (ppm)	1/Jv (10 ⁵) (s.m ² /m ³)	Cp (ppm)	1/Jv (10 ⁵) (s.m ² /m ³)	Cp (ppm)
Ph 4	5	1.0636	1.8860	1.2001	4.284	1.3501	7.3500
	6	0.9001	1.7500	1.0636	3.972	1.2001	6.8400
	7	0.7716	1.5840	0.9001	3.584	1.0636	6.4620
	8	0.5540	1.3420	0.7502	3.088	0.8251	5.4000
Ph 5	5	1.3501	0.7502	0.8251	3.712	0.8621	6.6420
	6	0.9747	0.7242	0.7502	3.420	0.8251	6.5820
	7	0.6752	0.4943	0.6807	3.300	0.6831	6.0180
	8	0.5999	0.4270	0.4933	2.852	0.6242	5.8260
Ph 6	5	1.3501	0.3930	1.6499	2.088	1.7250	4.9380
	6	0.9747	0.3830	0.9747	1.400	1.4999	4.5420
	7	0.6752	0.2150	0.9001	1.360	1.2001	4.1940
	8	0.5999	0.1940	0.7502	1.248	0.6925	2.9160

TABLE 4

Values of transfer parameters J_{diff} and C_{conv} for manganese salt

Ph	Concentration (ppm)	C _{conv} (ppm)	J _{diff} (10 ⁻⁵) (m ³ /s.m ²)
Ph 4	20 ppm	0.7478	1.1
	40 ppm	1.1590	2.6
	60 ppm	2.4198	1.0
Ph 5	20 ppm	0.2053	0.4
	40 ppm	1.6061	1.0
	60 ppm	3.5866	3.6
Ph 6	20 ppm	0.0408	0.3
	40 ppm	0.5035	1.0
	60 ppm	1.6691	1.9

Figures 8. Show the experimental results shown according to the equation. The salt content in permeate is represented by C_{conv}, and the diffusive flow is represented by J_{diff}, which is determined from the intercept and slope, respectively, for different concentrations at different pressures (Table 3). These results were equivalent to those reported by Y. A. Boussouga et al for the removal of various salts (NaCl, Na₂SO₄, MgSO₄) using Nanofiltration [69].

The equation was used to calculate the hydraulic permeability of pure water Lp (pure water = 1s.cm⁻¹) (4). Figure 6. Demonstrate the values of permeate flow Jv derived from various concentrations and Ph levels, as well as their fluctuations in terms of pressure P. By adjusting the trans-membrane pressure, we were able to achieve a linear development of the flow, demonstrating that Darcy's law is true.

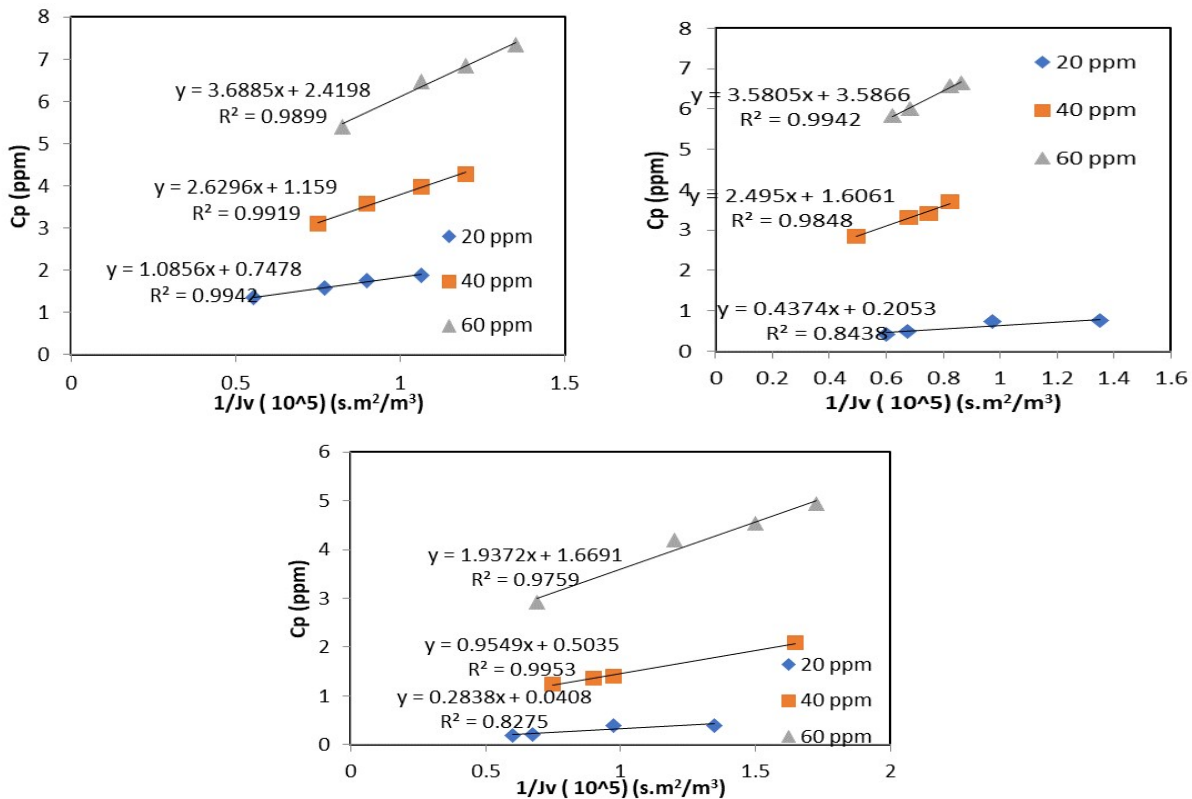


Figure 8: Cp Vs 1/Jv for different pressure & various Ph (a) Ph = 4 (b) Ph = 5 (c) Ph = 6

The slope of the curve indicates the critical pressure ($P_c =$), and the x-intercept shows the hydraulic permeability with the electrolyte solution L_p . Which of the following is the minimum pressure necessary for a permeate flow (Table 5). These results were equivalent to those reported by Y. A. Boussouga et al for the removal of various salts (NaCl , Na_2SO_4 , MgSO_4) using nanofiltration [69].

TABLE 5

The value of hydraulic permeability of manganese salt at different concentrations, different pressure & different Ph

Ph	Concentration (ppm)	L_p (10^{-6}) (L.cm ² / s.m ² .kg)	P_c (10^{-6}) (kg/cm ²)
Ph 4	20 ppm	2.7790	5.1856
	40 ppm	1.6700	0.3099
	60 ppm	1.5210	0.5697
Ph 5	20 ppm	3.4480	4.1620
	40 ppm	2.5810	1.6740
	60 ppm	1.5830	3.3180
Ph 6	20 ppm	3.4760	10.9090
	40 ppm	2.2660	4.5370
	60 ppm	2.6700	8.6175

IV. CONCLUSIONS

The influence of several operating factors such as applied pressure, feed concentration, and Ph on the separation of manganese ions from the effluent by the TFC NF-30 nanofiltration membrane was investigated in this study. Manganese ions were successfully removed using the Perma pilot size membrane system, and metal analysis was performed using normal procedures using an atomic absorption spectrophotometer (model SL-173). With increasing pressure (5 kg/cm², 6 kg/cm², 7 kg/cm², & 8 kg/cm²), the rejection coefficient for manganese ions increases. The rejection coefficient reduces as the manganese ion concentration in the feed (20 ppm, 40 ppm, and 60 ppm) increases at a constant flow rate. The influence of Ph (4, 5, and 6) was investigated, and it was discovered that the separation of manganese ions enhances as the Ph rises. For an initial feed concentration of 20 ppm, the maximum metal rejection was determined to be 99.03 %. In this work, the CFSK model was used to predict experimental rejection (R_{OE}) or real rejection and modeling rejection (R_{OM}) or observed rejection for manganese ions. The experimental and modeling rejection for manganese in the CFSK model is nearly equal to ± 0.03 . As a result, the CFSK model's projected values are more accurate.

V. ACKNOWLEDGEMENT

The corresponding author thanks AICTE, New Delhi, India, for funding research equipment through research proposal initiatives. (File No. 8023/BOR/RID/RPS/2009-10).

NOMENCLATURE

a_1 - $\sigma/(1-\sigma)$
 a_2 - $(1-\sigma)/PM$
 CA_i - Concentration of A at any position i (ppm)
 C_{conv} - solute concentration due to convection (mol/L)
 CF - Concentration of feed (ppm)
 C_p - Permeate Concentrate
 J_s - Solute volume flux (m³/s.m²)
 J_v - permeate volume flux (m³/s.m²)
 k - mass transfer coefficient (m/s)
 L_p - hydraulic permeability coefficient (L.cm²/s.m².kg)
 M_w - molecular weight
 PM - overall permeability coefficient (m/s)
 r - reflection coefficient
 R_o - observed rejection (%)

Greek letters

$\Delta\pi$ - osmotic pressure difference across the membrane (atm)
 σ - reflection coefficient

Subscript

A - Solute
 1 Feed solution
 2 Permeate solution
 conv - convection
 diff - diffusive
 f - feed
 M - membrane
 p - permeate
 s - solute
 sd - observed
 0- feed solution
 1- permeate solution

Superscript

f feed
 p permeate
 2- constant
 3- constant

VI. REFERENCES

1. Abdullah, N. Yusof, W.J. Lau, J. Jaafar, A.F. Ismail, Recent trends of heavy metal removal from water/wastewater by membrane technologies, Journal of Industrial and Engineering Chemistry, (2019) 76 17–38.
2. Q. Wang, Z. Xu, S. Wang, Z. Wang, J. Jia, H. Li, Y. Cao, Y. Chen, Y. Qin, F. Cui, Rapid synthesis of amorphous CoO nanosheets: A highly efficient catalyst for parachlorophenol degradation by peroxymonosulfate activation, Sep. Purif. Technol, (2021) 263 118369.
3. O. Bicak, Y. Ozturk, E. Ozdemir, Z. Ekmekci, Modelling effects of dissolved ions in process water

- on flotation performance, *Miner. Eng.* (2018) 128 84–91.
4. G. Li, X. Ma, R. Chen, Y. Yu, H. Tao, B. Shi, Field studies of manganese deposition and release in drinking water distribution systems: Insight into deposit control, *Water Res* (2019) 163 14897.
 5. M. Haddad, T. Ohkame, P.R. B'erub'e, B. Barbeau, Performance of thin-film composite hollow fiber nanofiltration for the removal of dissolved Mn, Fe and NOM from domestic groundwater supplies, *Water Res.* (2018) 145 408–417.
 6. L.-H. Cheng, Z.-Z. Xiong, S. Cai, D.-W. Li, X.-H. Xu, Aeration-manganese sand filter ultrafiltration to remove iron and manganese from water: Oxidation effect and fouling behavior of manganese sand coated film, *Journal of Water Process Engineering*, (2020) 38 101621.
 7. V.W. Hoyland, W.R. Knocke, J.O. Falkinham, A. Pruden, G. Singh, Effect of drinking water treatment process parameters on biological removal of manganese from surface water, *Water Res.* (2014) 66 31–39.
 8. Guidelines for drinking-water quality, in Recommendations, Volume 1, 3rd edition, World Health Organization, Geneva. (2008) 390 – 399.
 9. Sheth, Y., Dharaskar, S., Khalid, M., Sonawane, S, An environment-friendly approach for heavy metal removal from industrial wastewater using chitosan-based biosorbent: A review. *Sustainable Energy Technologies and Assessments*, (2021) 43 100951.
 10. Malkapuram, S. T., Sharma, V., Gumfekar, S. P., Sonawane, S., Sonawane, S., Boczkaj, G., Seepana. M. M., A review on recent advances in the application of biosurfactants in wastewater treatment. *Sustainable Energy Technologies and Assessments*, (2021) 48 101576.
 11. Bethi, B., Sonawane, S. H., Potoroko, I., Bhanvase, B. A., Sonawane, S. S., A novel hybrid system based on hydrodynamic cavitation for treatment of dye wastewater: The first report on the bench-scale study. *Journal of environmental chemical engineering*, (2017) 5(2) 1874-1884.
 12. Chandane, V. S., Rathod, A. P., Wasewar, K. L., Sonawane, S. S, Esterification of propionic acid with isopropyl alcohol over ion exchange resins: Optimization and kinetics. *Korean Journal of Chemical Engineering*, (2017) 34 (1) 249-258.
 13. Thakur, P., Sonawane, S. S., Application of nanofluids in CO₂ capture and extraction from wastewater. *Journal of Indian Association for Environmental Management (JIAEM)*, (2019) 39 (1-4) 4-8.
 14. Y. Bai, Y. Chang, J. Liang, C. Chen, J. Qu, Treatment of groundwater containing Mn (II), Fe (II), As (III) and Sb (III) by bio augmented quartz-sand filters, *Water Res.* (2016) 106 126–134.
 15. X. Tian, R. Zhang, T. Huang, G. Wen, The simultaneous removal of ammonium and manganese from surface water by MeOx: Side effect of ammonium presence on manganese removal, *Journal of Environmental Sciences* (2019) 77 346–353.
 16. X. Du, W. Yang, Y. Liu, W. Zhang, Z. Wang, J. Nie, G. Li, H. Liang, Removal of manganese, ferrous, and antibiotics from groundwater simultaneously using peroxymonosulfate-assisted in-situ oxidation/coagulation integrated with ceramic membrane process, *Sep. Purif. Technol.* (2020) 252 117492.
 17. G. Li, H. Hao, Y. Zhuang, Z. Wang, B. Shi, Powdered activated carbon enhanced Manganese(II) removal by chlorine oxidation, *Water Res.* (2019) 156 287–296.
 18. Y. Guo, T. Huang, G. Wen, X. Cao, The simultaneous removal of ammonium and manganese from groundwater by iron-manganese co-oxide filter film: The role of chemical catalytic oxidation for ammonium removal, *Chem. Eng. J.* (2017) 308 322–329.
 19. J.H. Bruins, Manganese Removal from Groundwater: Role of Biological PhysicoChemical Autocatalytic Processes, Delft University of Technology, (2016).
 20. J. Je'z-Walkowiak, Z. Dymaczewski, A. Szuster-Janiacyk, A.B. Nowicka, M. Szybowski, Efficiency of Mn removal of different filtration materials for groundwater treatment linking chemical and physical properties, *Water.* (2017) 9 498.
 21. S. Chaturvedi, P.N. Dave, Removal of iron for safe drinking water, *Desalination.* (2012) 303 1–11.
 22. M.S. Burger, S.S. Mercer, G.D. Shupe, G.A. Gagnon, Manganese removal during bench-scale biofiltration, *Water Res.* (2008) 42 4733–4742.
 23. Ejaz Haddadi, Jotiram G. Gujar, Shriram S. Sonawane, Kinetics and isotherm studies for adsorption of boron from water using titanium dioxide, *Canadian Journal of Chemical Engineering*, In Press, 2022, <https://doi.org/10.1002/cjce.24429>
 24. X. Du, G. Liu, F. Qu, K. Li, S. Shao, G. Li, H. Liang, Removal of iron, manganese, and ammonia from groundwater using a PAC-MBR system: the anti-pollution ability, microbial population, and membrane fouling, *Desalination.* (2017) 403 97–106.
 25. Ahmad, A. van der Wal, P. Bhattacharya, C.M. van Genuchten, Characteristics of Fe and Mn bearing precipitates generated by Fe(II) and Mn(II) co-oxidant with O₂, MnO₄ and HOCl in the presence of groundwater ions, *Water Res.* (2019) 161 505–516.
 26. K.-H. Choo, H. Lee, S.J. Choi, Iron, and manganese removal and membrane fouling during F in conjunction with prechlorination for drinking water treatment, *Journal of Membrane Science*, (2005) 267 18–26.
 27. D. Ellis, C. Bouchard, G. Lantagne, Removal of iron and manganese from groundwater by oxidation and microfiltration, *Desalination.* (2000) 130 255–264.
 28. S.L. Dashtban Kenari, B. Barbeau, Understanding ultrafiltration fouling of ceramic and polymeric membranes caused by oxidized iron and manganese in water treatment, *Journal of Membrane Science*, (2016) 516 1–12.
 29. X. Tang, J. Wang, H. Zhang, M. Yu, Y. Guo, G. Li, H. Liang, Respective role of iron and manganese in direct ultrafiltration: from membrane fouling to flux

- improvements, Separation and Purification Technology, (2020) 118174.
30. X. Tang, J. Qiao, J. Wang, K. Huang, Y. Guo, D. Xu, G. Li, H. Liang, Bio-cake layer based ultrafiltration in treating iron-and manganese-containing groundwater: Fast ripening and shock loading, *Chemosphere*. (2020) 128842.
 31. H. Wu, X. Xu, L. Shi, Y. Yin, L.-C. Zhang, Z. Wu, X. Duan, S. Wang, H. Sun, Manganese oxide integrated catalytic ceramic membrane for degradation of organic pollutants using sulfate radicals, *Water Res.* (2019) 167 115110.
 32. S.L. Dashtban Kenari, B. Barbeau, Understanding ultrafiltration fouling of ceramic and polymeric membranes caused by oxidized iron and manganese in water treatment, *Journal of Membrane Science*, (2016) 516 1–12.
 33. S.L. Dashtban Kenari, B. Barbeau, Integrated pyrolytic fluidized bed-membrane hybrid process for improved iron and manganese control in drinking water, *Water Res.* (2017) 113 50–61.
 34. Michal Bodzek, Krystyna Konieczny, Anna Kwiecińska, Application of membrane processes in drinking water treatment—state of art, *Desalination and Water Treatment*, (2011) 35 (1-3)164-184
 35. Deepti S Patil, Sanjay M Chavan, John U Kennedy Oubagaranadin, Studies on the removal of manganese from synthetic wastewaters by nanofiltration - A parametric and modeling study, *Desalination and Water Treatment*, (2017) 88 93-105
 36. N. Hilal, H. Al-Zoubi, N.A. Darwish, A.W. Mohammad, M. Abu Arabi, A comprehensive review of nanofiltration membranes: Treatment, pre-treatment, modeling, and atomic force microscopy, *Desalination*. (2004) 170 281-308.
 37. Ministry of Environment & Forests, Global good practices in industrial wastewater treatment and disposal/reuse, with special reference to common effluent treatment plants, Central Pollution Control Board, Govt. of India, 2015.
 38. Gadhe, A., Sonawane, S. S., Varma, M. N., Enhancement effect of hematite and nickel nanoparticles on biohydrogen production from dairy wastewater. *International Journal of Hydrogen Energy*, (2015) 40(13) 4502-4511.
 39. Gadhe, A., Sonawane, S. S., Varma, M. N., Influence of nickel and hematite nanoparticle powder on the production of biohydrogen from complex distillery wastewater in batch fermentation. *International Journal of Hydrogen Energy*, (2015) 40(34) 10734-10743.
 40. Sonawane, S. S., Gadhe, A., Thakur, P., Enhancement of the bio-hydrogen production from complex food wastewater using the hematite and nickel oxide nanoparticles. *Journal of Indian Association for Environmental Management (JIAEM)*, (2021) 41 (4) 45-51.
 41. Gadhe, A., Sonawane, S. S., Varma, M. N., Optimization of conditions for hydrogen production from complex dairy wastewater by anaerobic sludge using desirability function approach. *International Journal of Hydrogen Energy*, (2013) 38 (16) 6607-6617.
 42. Gadhe, A., Sonawane, S. S., Varma, M. N., Evaluation of ultrasonication as a treatment strategy for enhancement of biohydrogen production from complex distillery wastewater and process optimization. *International journal of hydrogen energy*, (2014) 39 (19) 10041-10050.
 43. Gadhe, A., Sonawane, S. S., Varma, M. N., Enhanced biohydrogen production from dark fermentation of complex dairy wastewater by sonolysis. *International Journal of Hydrogen Energy*, (2015) 40 (32) 9942-9951.
 44. Abhijit, G., Shriram, S., & Mahesh, V., Kinetic modeling of biohydrogen production from complex wastewater by anaerobic cultures. *Research Journal of Chemistry and Environment*, (2013) 17 (12) 129-135.
 45. Gülsev Soysüren, Ayşe Gül Yetgin, Özgür Arar, Müşerref Arda, Removal of manganese (II) from aqueous solution by ionic liquid impregnated polymeric sorbent and electrodeionization (EDI) techniques, *Process Safety and Environmental Protection*, (2022) 158 189-198.
 46. Mishra, S., Sonawane, S. S., Shimpi, N. G., Influence of organo-montmorillonite on mechanical and rheological properties of polyamide nanocomposites. *Applied Clay Science*, (2009) 46 (2), 222-225.
 47. Charde, S. J., Sonawane, S. S., Sonawane, S. H., Navin, S., Influence of functionalized calcium carbonate nanofillers on the properties of melt-extruded polycarbonate composites. *Chemical Engineering Communications*, (2018) 205 (4) 492-505.
 48. Shimpi, N. G., Kakade, R. U., Sonawane, S. S., Mali, A. D., Mishra, S., Influence of nano-inorganic particles on properties of epoxy nanocomposites. *Polymer-Plastics Technology and Engineering*, (2011) 50 (8), 758-761.
 49. Sonawane, S. S., Mishra, S., Shimpi, N. G., Effect of nano-CaCO₃ on mechanical and thermal properties of polyamide nanocomposites. *Polymer-Plastics Technology and Engineering*, (2009) 49 (1), 38-44.
 50. Sonawane, S. S., Mishra, S., Shimpi, N. G., Rathod, A. P., Wasewar, K. L., Comparative study of the mechanical and thermal properties of polyamide-66 filled with commercial and nano-Mg (OH)₂ particles. *Polymer-Plastics Technology and Engineering*, (2010) 49(5) 474-480.
 51. Sasidharan, S., Raj, S., Sonawane, S., Sonawane, S., Pinjari, D., Pandit, A. B., Saudagar, P., Nanomaterial synthesis: chemical and biological route and applications. In *Nanomaterials Synthesis* (2019) 27-51.
 52. Chandane, V. S., Rathod, A. P., Wasewar, K. L., Sonawane, S. S., Process optimization and kinetic modeling for esterification of propionic acid with benzyl alcohol on ion-exchange resin catalyst. *Korean*

- Journal of Chemical Engineering, (2017) 34 (4), 987-996.
53. Bart van der Bruggen, Nanofiltration, in Encyclopedia of Membrane Science and Technology, Eric M.V. Hoek and Volodymyr V. Tarabara, Ed., Belgium: John Wiley & Sons, (2013) 1-22.
 54. Bethi, B., Sonawane, S. H., Bhanvase, B. A., Sonawane, S. S., Textile industry wastewater treatment by cavitation combined with Fenton and ceramic nanofiltration membrane. Chemical Engineering and Processing-Process Intensification, (2021) 168 108540.
 55. N. Misdan, W.J. Lau, A.F. Ismail and T. Matsuura, Formation of thin film composite nanofiltration membrane: Effect of polysulfone substrate characteristics”, Desalination. (2013) 329 9–18.
 56. Sonawane, S., Thakur, P., Sonawane, S. H., Bhanvase, B. A., Nanomaterials for membrane synthesis: Introduction, mechanism, and challenges for wastewater treatment. In Handbook of Nanomaterials for Wastewater Treatment pp. (2021) 537-553.
 57. A. G. Boricha and Z. V. P. Murthy, Prediction of Nanofiltration performance by using membrane transport model for the separation of Nickel salts from aqueous solutions, Chemical product and process modeling, (2008) 3 (1) 1-23.
 58. R. García and A. P. Báez, Atomic Absorption Spectrometry (AAS), Atomic Absorption Spectroscopy, Dr. Muhammad Akhyar Farrukh (Ed.) (2012) 6-9.
 59. Z.V.P. Murthy and Latesh B. Chaudhari, Application of nanofiltration for the rejection of nickel ions from aqueous solutions and estimation of membrane transport parameters, Journal of Hazardous Materials, (2008) 160 70–77.
 60. Rupali R. Bhutale, S.M.Chavan, J.G.Gujar, D.S.Patil, Application of Nanofiltration for the rejection of chromium ions from synthetic water, International journal of science Technology & Engineering, (2018) 5 (1) 54-59.
 61. Norherdawati Kasim, Abdul Wahab Mohammad, Siti Rozaimah Sheikh Abdullah, Iron and Manganese removal by Nanofiltration and Ultrafiltration membranes: influence of pH adjustment, Malaysian Journal of Analytical Sciences (2017) 21 (1) 149 – 158.
 62. B.A.M. A-Rashdi, D.J. Johnson, N. Hilal, Removal of heavy metal ions by Nanofiltration, Desalination. (2012) 1-16.
 63. Jesús M. Arsuaga, M.J. López Muñoz, José Aguado, Arcadio Sotto, Temperature, pH and concentration effects on retention and transport of organic pollutants across thin-film composite nanofiltration membranes, Desalination. (2008) 221 253-258.
 64. J. G. Wijmans, R.W. Baker, The solution-diffusion model: a review, Journal of Membrane Science, (1995) 107 1–21.
 65. Z.V.P. Murthy and Latesh B. Chaudhari, Application of nanofiltration for the rejection of nickel ions from aqueous solutions and estimation of membrane transport parameters, Journal of Hazardous Materials, (2008) 160 70–77.
 66. B.A.M. A-Rashdi, D.J. Johnson, N. Hilal, Removal of heavy metal ions by Nanofiltration, Desalination. (2012) 1-16.
 67. H. Al-Zoubi, N. Hilal, N.A. Darwish and A.W. Mohammad, Rejection and modeling of sulfate and potassium salts by nanofiltration membranes: neural network and Spiegler–Kedem model, Desalination. (2007) 206 42-60.
 68. Y.A. Boussouga, A. Lhassani, Study of mass transfer mechanisms for reverse osmosis and nanofiltration membranes intended for desalination, Journal of Materials and Environmental Sciences, (2017) 8 (3) 1128-1138.
 69. E.A.Mason, H.K. Lonsdale, Statistical–mechanical theory of membrane Transport, Journal of Membrane Science, (1990) 511– 81.